Chemical Science

ROYAL SOCIETY OF CHEMISTRY

EDGE ARTICLE

View Article Online
View Journal | View Issue

Cite this: *Chem. Sci.*, 2024, **15**, 9842

All publication charges for this article have been paid for by the Royal Society of Chemistry

Carbonyl mediated fluorescence in aceno[*n*] helicenones and fluoreno[*n*]helicenes†

Michal Šámal,*[a] Ludmilla Sturm,[b] Marzena Banasiewicz,[c] Irena Deperasinska,[c] Boleslaw Kozankiewicz,[c] Olaf Morawski,[c] Yuuya Nagata,[d] Pierre Dechambenoit,[b] Harald Bock,[b] Amandine Rossel,[b] Miloš Buděšínský,[a] Anthony Boudier[e] and Andrej Jančařík*[b]

Received 5th February 2024
Accepted 19th April 2024

DOI: 10.1039/d4sc00892h

rsc.li/chemical-science

Helicenes are very attractive chiral non-planar polycyclic aromatic hydrocarbons possessing strong chiroptical properties. However, most of the helicenes absorb light mainly in the ultraviolet region, with only a small segment in the blue part of the visible spectrum. Furthermore, carbo[*n*]helicenes exhibit only weak luminescence that limits their utilization. Herein, we demonstrate that peripheral decoration of the helicene backbone with an aryl-carbonyl group shifts the absorption to the visible region and simultaneously improves their fluorescence quantum yields. We thus show that the carbonyl group, commonly considered as detrimental to emission, has the capability of improving optical and photophysical properties. Two different families, aceno[*n*]helicenones and fluoreno[*n*]helicenes, are presented with comprehensive spectrochemical characterization. TD-DFT calculations were implemented to clarify their electronic profiles. We show that increasing the helical length in aceno[*n*]helicenes increases absorption onset, g_{abs} and g_{lum}. Extension of the peripheral aromatic part in fluoreno[*n*]helicenes leads to a blue shift in both absorption and emission.

Introduction

The introduction of a carbonyl group into the aromatic skeleton significantly reduces the HOMO–LUMO gap which is an essential parameter in organic electronics. This effect is often evident by a shift of the absorption and the emission into the visible region. Even relatively short conjugated carbonyl systems are capable of absorption of long-wavelength parts of the visible spectrum. However, carbonyl groups are generally considered as detrimental to the fluorescence quantum yield.[1] This is due to efficient intersystem crossing (ISC) between singlet and triplet excited manifolds of nπ* and ππ* character. The ISC yield of aromatic ketones is related simultaneously to the very small energetic singlet-triplet gap (<0.2 eV) due to the orthogonal orientation between non-bonding *n* and anti-bonding π* orbitals and to the strong spin–orbit coupling following El-Sayed's rule.[2] Therefore, most aromatic ketones undergo extremely fast ISC within picoseconds, *e.g.* benzophenone: 5–10 ps,[3] xanthone: 2 ps,[4] anthrone: 70 ps.[5] This results from the proviso that systems which possess low lying singlet ^{1}nπ* or ^{1}ππ* (S1 and potentially S2) states are coupled with triplet states of similar energy and, intrinsically, different symmetry (^{3}ππ* or ^{1}nπ*, respectively).[2] For this reason, the integration of a carbonyl group into the aromatic system would seem counter-intuitive for the purpose of improving the photophysical properties. Thus, the carbonyl group is rarely considered beneficial for the luminescence. Herein we show that the installation of an aryl-carbonyl group at the periphery of the carbo[*n*]helicene helix not only shifts the absorption by more than 100 nm (>4270 cm^{-1}) but also significantly increases the fluorescence quantum yield (Φ_F) when compared to pristine carbo[*n*]helicenes. Although helicenes are known to exhibit very remarkable chiroptical properties such as high optical rotations (>±1000), circular dichroism, circularly polarized luminescence and nonlinear optical activity,[6] they show only weak luminescence: the fluorescence quantum yield (Φ_F) of [6]helicene is $\Phi_F = 0.04$, [7]helicene $\Phi_F = 0.02$ and [*n*]helicene (where $n \geq 8$) $\Phi_F \leq 0.01$.[7] This is mainly due to the small oscillator strength and to significant intersystem crossing (ISC).[8] Furthermore, the absorption onset wavelength (λ_{onset}) of helicenes increases initially with increasing length but saturates around 490 nm ([11]helicene). Thus, pristine carbo[*n*]helicenes are colorless (*n*

[a]*Institute of Organic Chemistry and Biochemistry of the Czech Academy of Sciences, 166 10 Prague 6, Czech Republic. E-mail: samal@uochb.cas.cz*

[b]*Université de Bordeaux, CNRS, Centre de Recherche Paul Pascal, CRPP, UMR 5031, 33600 Pessac, France. E-mail: andrej.jancarik@crpp.cnrs.fr*

[c]*Institute of Physics, Polish Academy of Sciences, Al. Lotników 32/46, 02-668 Warsaw, Poland*

[d]*Japan Institute for Chemical Reaction Design and Discovery (WPI-ICReDD), Hokkaido University, Sapporo, Hokkaido 001-0021, Japan*

[e]*Institut de Chimie et Biologie des Membranes et des Nanoobjets (CBMN), Université de Bordeaux-INP, UMR 5248, Allée St Hilaire, 33607, Pessac Cedex, France*

† Electronic supplementary information (ESI) available. CCDC 2295945–2295947. For ESI and crystallographic data in CIF or other electronic format see DOI: https://doi.org/10.1039/d4sc00892h

≤ 6) or yellow ($n \geq 7$) substances. In order to qualify helicenes for use in various luminescence-based (chiropto)electronic applications such as fluorescent probes, signaling systems, OLEDs, bioimaging *etc.*, it is necessary to improve their luminescence quantum yields and modulate their absorption/emission (HOMO–LUMO gap) on demand. To improve photochemical parameters with emphasis on Φ_F, a number of different approaches have been employed,[9] such as substitution, hetero-doping, lateral extension, or metal complexation.

Crassous, Favereau, Autschbach and coworkers have shown that the functionalization of [6]helicene allows the modulation of the circularly polarized luminescence, the absorption onset and the fluorescence quantum yield (Fig. 1B).[10,11] Matsuda, Hirose *et al.* have developed [7]helicene derivatives with enhanced circularly polarized luminescence and improved fluorescence quantum yields (Fig. 1C).[12] In the case of helicenes longer than [7]helicene, only theoretical studies have been conducted to investigate their chiroptical properties. It was shown that the dissymmetry factor of carbo[*n*]helicenes increases with the helix length *n*.[14] Recently, Narita, Müllen, Pieters and coworkers have demonstrated that a small increase (from $n = 7$ to 9) of the helix length in laterally extended [*n*]helicenes can lead to a 10-fold increase of the dissymmetry factor (Fig. 1D).[13] Herein, we show that the carbonyl group can do the job of increasing Φ_F while simultaneously shifting the absorption onset to longer wavelengths. It is striking that although many helicenes bearing a carbonyl moiety have been described, all of them are orange/red solids which exhibit no or very weak fluorescence.[15–19] The non-emissivity was always attributed to the carbonyl group. Thus fluorenone-fused helicenes have been extensively used only as precursors to synthesize a variety of highly luminescent helicene-like materials such as fluorene-fused helicenes,[15,16] azahelicenes[20] or indenofluorenes.[21,22] In this study we show that installation of fluorenone or acenone units at the periphery of the helicene (Fig. 2) has a very positive effect on their photophysical properties. The absorptions and emissions are shifted into the visible region and the fluorescence quantum yields are greatly enhanced. In addition, our study demonstrates that the established rule that the carbonyl group is detrimental to such properties has important limitations. We show that the carbonyl group can indeed improve the optical and photophysical properties. Furthermore, we show that the absorption and luminescence dissymmetry factors (g_{abs} and g_{lum}) in the obtained systems strongly depend on the helix length *n*, in contrast to pristine helicenes.

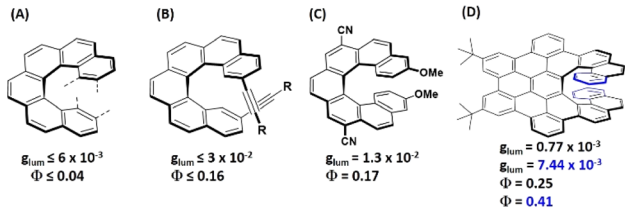

Fig. 1 Luminescent properties of helicenes and their derivatives.

Results and discussion

For this study we have designed and synthesized two families of carbo[*n*]helicenes. The first family, aceno[*n*]helicenones **1A–8A** (Fig. 2 and 3), are helicenes that are peripherally annulated *via* an aryl-carbonyl group that formally creates an acene unit. The second family, fluoreno[*n*]helicenes **1F–8F**, is annulated such that a fluorenone unit is inserted into the helicene backbone. Installing an aromatic carbonyl group in this way at the periphery of the helicene scaffold has a significant effect on the

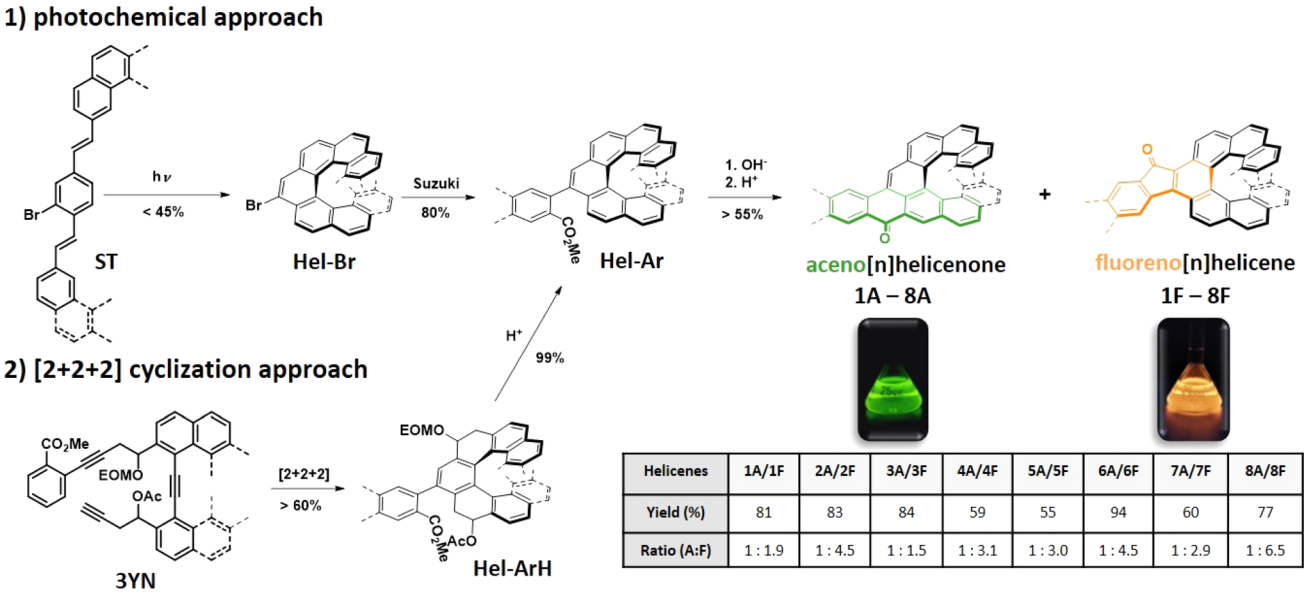

Helicenes	1A/1F	2A/2F	3A/3F	4A/4F	5A/5F	6A/6F	7A/7F	8A/8F
Yield (%)	81	83	84	59	55	94	60	77
Ratio (A:F)	1 : 1.9	1 : 4.5	1 : 1.5	1 : 3.1	1 : 3.0	1 : 4.5	1 : 2.9	1 : 6.5

Fig. 2 Synthesis of aceno[*n*]helicenones **1A–8A** and fluoreno[*n*]helicenes **1F–8F**; structures of **1A–8A**/**1F–8F** are shown in Fig. 3, EOM = ethoxymethyl ether.

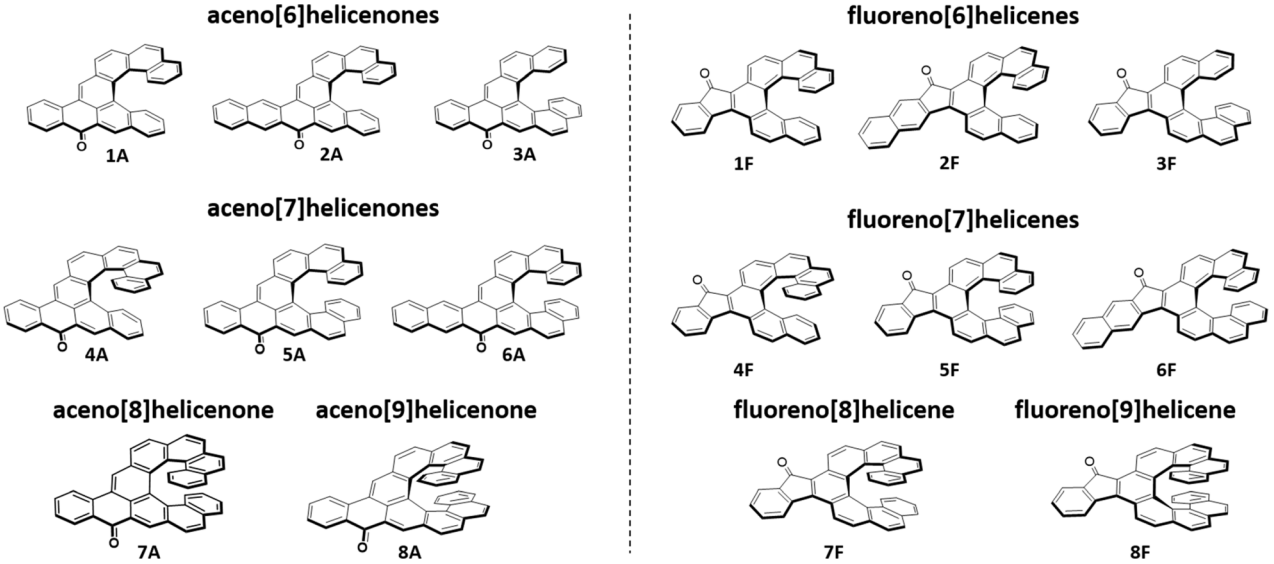

Fig. 3 List of aceno[*n*]helicenones **1A–8A** and fluoreno[*n*]helicenes **1F–8F**.

optical properties of the studied helicenes. For example, the absorption is shifted to the visible region by more than 50 nm (2160–3370 cm^{-1}) in the aceno[*n*]helicenone family and more than 100 nm (4270–6000 cm^{-1}) in the fluoreno-derivatives, and the fluorescence quantum yields are increased up to six times when compared to the pristine helicenes. We have deployed two versatile approaches providing aceno-/fluoreno[*n*]helicenone series **1A–8A**/**1F–8F** (Fig. 2).

The first approach is based on the Mallory photo-cyclization of suitable bromo-stilbene precursors **ST** (prepared by Wittig reaction) providing directly bromo-helicenes **Hel-Br**. The bromo atom fulfils two crucial functions that are (1) deactivation of the *ortho*-position against photocyclization and thus directing the cyclization toward the helicene and (2) being a coupling partner in a subsequent Suzuki reaction. The second approach is based on [2 + 2 + 2] cycloisomerization of suitable tri-ynes **3YN**, developed by I. Stará and I. Starý *et al.*[23] Intramolecular cyclization (catalyzed by a Co^{I} catalyst) followed by elimination/aromatization provides directly arylated helicenes **Hel-Ar** bearing carboxylic ester group. Basic hydrolysis of the ester group leads to the acids. The helicenic esters **Hel-Ar** and their corresponding acids consist of two unseparable atropodiastereomers (for details, see ESI† page S158). The final acid-catalyzed cyclization afforded aceno[*n*]helicenones and fluoreno[*n*]helicenes **1A–8A**/**1F–8F** simultaneously in ratios varying between 1 : 1 and 1 : 7. The fluoreno[*n*]helicenes were always formed preferentially. The density functional theory (DFT) calculations at the level of the ωB97X-D/Def2SVP on the formation process of **1A** and **1F** suggested that one atropodiastereomer preferentially produces **1F**, while the other atropodiastereomer affords a mixture of **1A** and **1F** (see ESI† page S189). This result of the calculation showed a good agreement with the experimental outcomes and corroborates that fluoreno[*n*]helicenones are formed preferentially. The significant difference in polarity of aceno[*n*]helicenones and fluoreno[*n*]helicenes allows us to very effectively separate the two helicenes by traditional column chromatography. All the final structures are well soluble in common organic solvents, and thus they were characterized by proton and carbon nuclear magnetic resonance spectroscopy (^{1}H and ^{13}C NMR) and high-resolution mass spectrometry (HR-MS). In addition, the structures of the fluoreno[*n*]helicenes **5F**, **6F** and **8F** were unambiguously confirmed by single crystal X-ray diffraction (for details, see ESI† page S165).

Photophysical and electrochemical properties of aceno[*n*] helicenones 1A–8A

The structures of the series have been designed in order to systematically study how the length of the helicene and acene parts will affect their absorption/emission and their chiroptical properties such as electronic circular dichroism (ECD), circularly polarized luminescence (CPL) and optical rotatory power. Isoelectronic aceno[*n*]helicenones **4A** and **5A** are unique systems which differ in the position of Clar sextets and in the position of a double bond relative to the carbonyl group (in blue color, Fig. 5a and b). This reveals the relation of the geometry with the physicochemical properties. First, aceno[*n*]helicenones **3A**, **5A**, **7A** and **8A** have been investigated to probe the effect of the helicene length on absorption and emission (Table 1). The ultraviolet-visible (UV-Vis) absorption and photoluminescence (PL) spectra were recorded first in nonpolar hexane (10^{-5} M) (as a representative example of **5A**, Fig. 4). The electronic absorption spectra of **3A**, **5A**, **7A** and **8A** cover the entire ultraviolet region and a major part of the blue region with a maximum located at 460 nm, 480 nm, 489 nm and 504 nm, respectively.

These absorption maxima located in the visible light region render these compounds orange. The absorption maximum is red-shifting with each further benzene annulation. A major increase is observed when going from aceno[6]helicenone **3A** to aceno[7]helicenone **5A**, which is most likely related to the fact that the two terminal rings of the [7]helicene backbone of **5A** overlap. This overlap brings additional through-space conjugation and a perceptibly red-shifted absorption. This aceno[*n*]

Table 1 The evolution of the photophysical properties upon elongation of the helix

Helicene	$\lambda_{(onset)}$ [nm] hexane	$\lambda_{(em)}$ [nm] DCM	B_{CPL}[c]	g_{lum}[d] (10^{-3}) DCM (hexane)	$[\alpha]_D^{20}$ DCM	Φ_{PL}[e] (%) hexane/DCM/	E_{HOMO}[f] [eV]	E_{LUMO}[g] [eV]
lA	469	513[a]	6.6	+1.7 −1.5	+2147 −2167	3.6/12.5/11.4	−5.89	−3.21
2A	475	534[a]	1.0	+0.58 −0.52	+770 −748	5.0/8.3/7.6	−5.88	−3.23
3A	467	494[a]	2.9	+1.2 −1.0	+1094 −1031	1.3/8.5/7.8	−5.95	−3.27
4A	481	520[b]	6.0	+3.0 −2.9	+3493 −3526	3.4/8.3/7.6	−5.82	−3.2
5A	493	530[a]	4.3	+2.0 −2.0	+3620 −3672	3.3/6.6/5.8	−5.78	−3.23
6A	497	546[a]	2.5	+0.82 −0.80	+2014 −1945	7.9/11.2/10.8	−5.78	−3.23
7A	501	538[a]	3.9	+3.0 −3.1	+4789 −4633	4.0/4.9/6.8	−5.74	−3.23
8A	517	555[a]	12.3	+6.2 (−7.8) −6.1 (8.0)	+6015 −6297	5.1/6.4/4.9	−5.68	−3.25

[a] Wavelength of excitation 330 nm. [b] Wavelength of excitation 336 nm. [c] Brightness calculated as $B_{CPL} = \varepsilon_{max} \times \Phi_{PL} \times |g_{lum}|/2$. [d] Concentration $c \approx 1 \times 10^{-5}$ M. [e] Measured at room temperature ($c \approx 1 \times 10^{-6}$ M). [f] Calculated as $E_{HOMO} = E_{LUMO} - E_{(0,0)}$. [g] Calculated using the equation $E_{LUMO} = -[E'_{red/onset} + 4.8]$ referenced against Fc/Fc^+.[24]

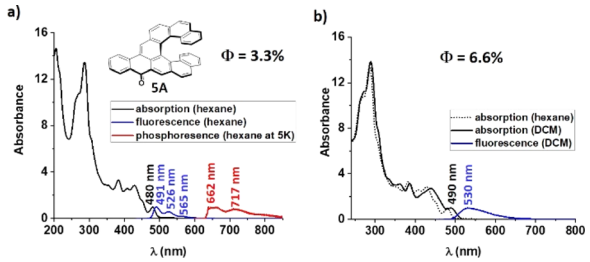

Fig. 4 Absorption and emission spectra of **5A** in (a) hexane (b) dichloromethane, ($c \approx 1 \times 10^{-5}$ M).

helicenone series follows a regular trend of decrease of the gap ($E_{0,0}$) with increase of the length of the π-system (for details, see ESI† Table S1, page S147 and S158). The lowest absorption bands arise from the allowed π → π* transitions with high oscillator strengths ($f = 0.43$ for **3A**; $f = 0.19$ for **5A**; $f = 0.16$ for **7A** and $f = 0.16$ for **8A**) and correspond mainly to $S_0 \rightarrow S_1$ transitions. In nonpolar hexane, the fluorescence spectra of the **1A–8A** series show a well-structured vibrational emission band which can be ascribed to a locally excited (LE) state character. Very small Stokes shifts (≤530 cm^{-1}, ≤11 nm) are pointing to small changes of the electron distributions in the ground and excited states. In all cases of aceno-derivatives **1A–8A**, solvatofluorochromism was observed. The polarity of the environment has only a limited effect on the absorption, causing a small red-shift of the long-wavelength absorption bands. However, passing from low-polarity hexane to polar dichloromethane (DCM) or acetonitrile (ACN) has a pronounced effect on the emission spectra. There is a notable disappearance of the vibrational features of the emission band, accompanied by a strong red-shift. Such large Stokes shifts (1220–2420 cm^{-1}, 30–60 nm) indicate that the dipole moment of low-lying excited states (S_1) is larger than in the ground state (S_0). According to the calculation results, the dipole moments of aceno-helicenes **1A–8A** in the ground state are of the order of 4–5 D, and in the excited state 8–12 D, which corroborate to the experimentally observed Stokes shifts with increasing of solvent polarity (for details, see ESI† page S163). This difference of dipole moments characterizes an electron–donor–acceptor (EDA) system. In our case, the carbonyl group behaves as an acceptor unit owing to its strong electron-withdrawing effect, and the electron rich helicene wing functions as a donor. This electron flow is visible in the electron density distribution of HOMO and LUMO, obtained by density functional theory (DFT) and time-dependent DFT (TD-DFT) calculations based on B3LYP functional and 6-31g(d) basis set. Although the HOMO and LUMO are extended over the whole molecule, the main density of the HOMO is located on the helicene wing and the main density of the LUMO is distributed over the carbonyl-acene part (Fig. 5a and b). Moreover, the symmetry of these orbitals, compared to the orbitals of the parent helicene, is disturbed and causes a clear

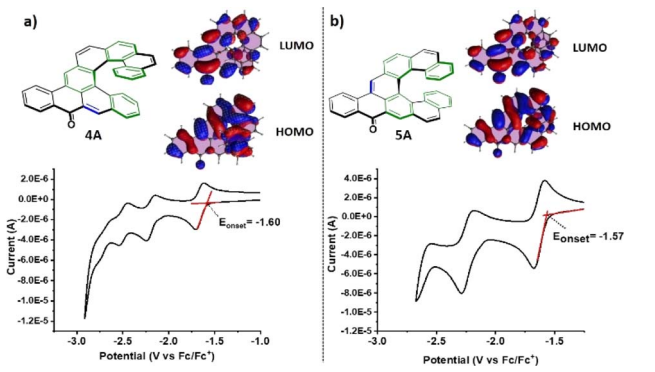

Fig. 5 (a) Electronic configuration of **4A** and its cyclic voltammogram (b) electronic configuration of **5A** and its cyclic voltammogram.

increase in oscillator strengths for the transitions between the S_0 and S_1 states (for details see ESI† page S162). This is accompanied by an increase in the fluorescence yield of aceno-helicenes **1A–8A**. However, the fluorescence yield is limited by non-radiative intersystem crossing processes taking place by different channels, *i.e.* to the numerous triplet states with energies close to that of the S_1 state. However, the effect is less prominent as the length of the helix increases. For instance, there is a six-fold Φ_F increase in a case of aceno[6]helicenone **3A** in polar DCM ($\Phi_F = 0.085$) or ACN ($\Phi_F = 0.078$), when compared to the value in nonpolar hexane ($\Phi_F = 0.013$), while for aceno[9] helicenone the Φ_F are comparable in nonpolar or polar environment (for details see the Table 1 and S147†). The emission is characterized by short fluorescence lifetimes (2–4 ns) of all the aceno-derivatives **1A–8A**, much shorter than the lifetimes of the corresponding [*n*]helicenes (10–15 ns).[25] In the next step, we have investigated effect of the acene length on the photophysical properties. For this purpose, the aceno-derivatives **1A**, **2A**, **5A** and **6A** were synthesized. In the acene series, the absorption maximum systematically increases by *ca.* 100 nm with each additional benzene ring.[26,27] In contrast, increasing the length of the acene part in the aceno[*n*]helicenones by one benzene ring leads to a smaller bathochromic shift than the one caused by an increase in the length of the helicene part. A linear one-benzene ring annulation of the acene part red-shifts the absorption maximum by only 4 nm (**1A** → **2A**, 459 nm → 463 nm or **5A** → **6A**, 480 nm → 484 nm), whereas elongation of the helicene part by one benzene ring red-shifts the absorption maximum by 9 nm (**1A** → **4A**, 459 nm → 468 nm or **5A** → **7A**, 480 nm → 489 nm). We assume that this is due to the extra through-space conjugation caused by the overlap of the terminal helicene rings. Linear benzannullation of the acene part increases the Φ_F of **2A** and **6A** in nonpolar hexane (Φ_F of **1A** → **2A**: 0.036 → 0.050 and **5A** → **6A**: 0.033 → 0.079). The fluorescence quantum yield of **2A** decreases but that of **6A** increases in polar DCM (Φ_F of **1A** → **2A**, 0.125 → 0.083 and **5A** → **6A**, 0.066 → 0.112). Last but not least, the isoelectronic derivatives **4A** and **5A** allow us to study the relation between the geometry and the physicochemical properties. Both structures are composed of tetracene and [7]helicene units. They differ in the position of the ring with double bond character (in blue color, Fig. 5a and b) relative to the carbonyl group. This position can be controlled by the arrangement of the tetracene and [7] helicene units and thus by localization of the Clar π-sextets in the helicene part (green color, Fig. 5a and b). The position and thus the conjugation of the double bond to the carbonyl group may affect the physicochemical properties of the whole aromatic system. It can also have consequences for the chemical reactivity, for instance **4A** and **5A** may behave differently upon nucleophilic attack (1,2- *vs.* 1,4-addition).[28,29] We found that most of the photophysical and chiroptical properties of **4A** and **5A** are comparable and only the absorbance maxima of **5A** (480 nm, double bond in *para*-position to the carbonyl) is red-shifted by 12 nm when compared to **4A** (468 nm, double bond in *ortho*-position to the carbonyl). However, the geometry strongly affects the redox behavior, as evidenced by cyclic voltammetry (CV).

All the aceno-derivatives **1A–8A** exhibit weak phosphorescence in hexane at 5 K, but this emission is absent in DCM. The phosphorescence emission band has two maxima in the 600–800 nm range. The singlet–triplet gap (ΔE_{S0-T1}) was determined from the fluorescence and phosphorescence onset wavelengths. Plotting the singlet-triplet gaps (ΔE_{T1-S0}) of the aceno[*n*]helicenones **3A**, **5A**, **7A** and **8A** we observed a systematic decrease with increasing length of the helicene part, which confirms that the energy of the triplet state is associated with conjugation length (see ESI† page S158). Likewise, the energy gap ΔE_{S1-T1} between the lowest excited singlet (S_1) and triplet (T_1) states decreases with increasing length of the helicene part. Surprisingly, elongation of the acene part (**1A** → **2A** or **5A** → **6A**) leads to an increase of the gap ΔE_{S0-T1}, in stark contrast to the pristine acenes.[30] The energy-state level diagrams of **1A–8A** were obtained by TD-DFT calculations. All energy diagrams exhibit that higher triplet states (T_3, T_4 and potentially T_5) are energetically close ($\Delta E_{S1-T4/3} \leq 0.1$ eV) to the S_1 state and may constitute a main channel for non-radiative intersystem crossing (ISC, $S_1 \rightarrow T_n$). The resulting population of the T_1 state (by non-radiative $T_n \rightarrow T_1$) is manifested by the emission of phosphorescence. The efficient ISC (together with the nonradiative internal conversion, $S_1 \rightarrow S_0$) compete with the radiative depopulation of the S_1 state, and the result is reduced quantum yield of the fluorescence emission.

Cyclic voltammetry (CV) measurements were performed in acetonitrile to determine the redox properties of **1A–8A**. All exhibit two reduction processes, except for **4A** and **8A**, which exhibit three reversible reductions. The first reductions show sharp reversible waves with half-wave potentials around $E_{1/2}^{red} \approx -1.5$ V (for details, see ESI†). The second reduction is irreversible, except for **4A** and **8A**. **1A–8A** all do not show any oxidation wave below +1.0 V (*vs.* Fc/Fc^+), suggesting a poor electron donating ability of the helicene wing. As already mentioned, isoelectronic **4A** and **5A** differ only in the position of the double bond (blue color, Fig. 5a and b) relative to the carbonyl group (*para*-/*ortho*-, determined by Clar's aromatic sextets). Interestingly, the systems with a double bond adjacent to the carbonyl group (**4A** and **8A**) exhibit reversible three electron reductions with $E_{1/2}^{red} = -1.66$ V, −2.20 V and −2.50 V for **4A** and −1.62 V, −2.16 V and −2.53 V for **8A** (*vs.* Fc/Fc^+). This particular geometry renders the doubly reduced species stable at the time scale of the CV. We suppose that the stability of the species after two single electron reductions of **4A** and **8A** implies that they contain same number of Clar π-sextets (for details, see ESI† page S164). From the onset of the reduction wave, the LUMO energy levels of **1A–8A** were calculated. The HOMO energy levels were calculated from the wavelength of the absorption onset.

Chiroptical properties of aceno[*n*]helicenones 1A–8A

To investigate chiroptical properties of the aceno[*n*]helicenones **1A–8A**, the racemic mixtures were resolved into their corresponding enantiomers by HPLC on a chiral stationary phase column. The absolute configurations were assigned by circular dichroism (CD) spectroscopy with the aid of TD-DFT calculations at the level of CAM-B3LYP/Def2TZVP//CAM-B3LYP/

Def2SVP with solvent effect (for details, see ESI† page S159–S161). In all cases the first eluting fraction was assigned as the *P*-(+) and the second one as *M*-(−) enantiomer. **1A–8A** all show perfect mirror image CD spectra with strong opposite Cotton effects (see **5A** as a representative example in Fig. 6a). The *P*-(+) enantiomers of **3A**, **5A**, **7A** and **8A** show a dominant positive Cotton effect in their CD spectra with maximum at 360 nm, 387 nm, 402 and 414 nm, respectively. These positive absorption bands were assigned to $S_0 \rightarrow S_{4-6}$ transitions. All the aceno-derivatives exhibit large absorption dissymmetry factors (g_{abs}) in the range of 3.2×10^{-3}–13.6×10^{-3} (for details see ESI,† page S131–S153). The g_{abs} increases as the length of the helicene increases. There is a two-fold increase of the g_{abs} when going from tetraceno[6]helicenone **3A** ($g_{abs} = 6.0 \times 10^{-3}$) to tetraceno [9]helicenone **8A** ($g_{abs} = 13.6 \times 10^{-3}$). In contrast, the g_{abs} decreases as the length of the acene part increases (**1A** → **2A**, $g_{abs} = 4.5 \times 10^{-3} \rightarrow 1.9 \times 10^{-3}$; **5A** → **6A**, $g_{abs} = 10.0 \times 10^{-3} \rightarrow 6.0 \times 10^{-3}$). All the aceno-derivatives **1A–8A** show mirror-image CPL spectra and the sign of the CPL matches that of the CD of the corresponding transition. Based on theory,[31] the luminescence dissymmetry factor (g_{lum}) of pristine carbo[*n*]helicenes should increase as the extension of the helix increases. Our calculations and experimental data confirm the same upward trend in aceno[*n*]helicenones. The g_{lum} values of **3A**, **5A**, **7A** and **8A** derivatives were as follows: ***P*-3A**, $g_{lum} = 1.2 \times 10^{-3}$; ***P*-5A**, $g_{lum} = 2.0 \times 10^{-3}$; ***P*-7A**, $g_{lum} = 3.0 \times 10^{-3}$; ***P*-8A**, $g_{lum} = 6.2 \times 10^{-3}$. The polar environment induces an excited CT state in the aceno[*n*]helicenones **1A–8A**. Since the CPL reflects the structure of the emissive excited state, we have probed and compared the CPL of the **8A** in nonpolar cyclohexane (favoring a LE state) and polar DCM (favoring a CT or a HLCT state). The g_{lum} value of ***P*-8A** in nonpolar cyclohexane (8.0×10^{-3}) was significantly increased when compared to the polar DCM (6.2×10^{-3}). Lengthening of the acene part substantially decreases the g_{lum} value (***P*-1A** → ***P*-2A**, $g_{lum} = 1.7 \times 10^{-3} \rightarrow 0.58 \times 10^{-3}$; ***P*-5A** → ***P*-6A**, $g_{lum} = 2.0 \times 10^{-3} \rightarrow 0.82 \times 10^{-3}$). The rotatory power of **1A–8A** is lower when compared to the parent carbo[*n*]helicenes, but with a similar trend, *i.e.* the specific rotation is increasing with extension of the helix. For instance, the specific rotation is increased by a factor of six when going from [6]helicene ***P*-3A** (+1094 deg cm^2 g^{-1}) to [9]helicene ***P*-8A** (+6015 deg cm^2 g^{-1}). The lengthening of the acene part has the opposite effect, *i.e.* the specific rotation is decreasing with the length of the acene part (***P*-1A** → ***P*-2A**, +2147 → +770 deg cm^2 g^{-1}; ***P*-5A** → ***P*-6A**, +3620 → +2014 deg cm^2 g^{-1}).

Photophysical and electrochemical properties of fluoreno[*n*] helicenes 1F–8F

The absorption onset of the fluoreno[*n*]helicenes **1F–8F** is located at longer wavelengths than 500 nm, which makes them red in the solid state (Fig. 7). The absorption onset is systematically red-shifted with each benzannulation of the helix. There is increase an of 54 nm when going form [6]helicene **3F** to [9] helicene **8F** (**3F** $\lambda_{onset} = 534$ nm, **5F** $\lambda_{onset} = 549$ nm, **7F** $\lambda_{onset} = 560$ nm, **8F** $\lambda_{onset} = 588$ nm). Interestingly, the biggest increment (28 nm) is observed when going from [8]helicene **7F** to [9] helicene **8F** and not when going from [6]helicene **3F** to [7]helicene **5F**, where the terminal rings start to overlap and extra through space-conjugation appears. Unfortunately, we do not have a satisfying explanation for that observation at this moment. The longest absorption band (assigned to $\pi \rightarrow \pi^*$) of the fluoreno-derivatives is broad and featureless, except for **2F**, **3F** and **6F**, whose spectra are more structured.

While the absorption spectra of **2F**, **3F** and **6F** red-shift and broaden with increasing polarity, those of the other fluoreno homologs are not modified by changing the polarity of the environment, suggesting that there are no significant changes of the electron distributions in the ground state. The emission spectra of **1F–8F** are broad (spanning over 200 nm) with two weakly visible maxima in nonpolar hexane. The emission spectra in polar DCM are broad and featureless with very large Stokes shifts (2730–5350 cm^{-1}). This suggests that the excited state S_1 has partial LE character in a low-polar environment and CT character in a polar media. In this system the fluorenone substructure behaves as an acceptor group owing to the strong electron-withdrawing effect of the carbonyl, and the electron rich helicene wings behave as a donor. **1F–8F** all exhibit moderate fluorescence in nonpolar hexane and very weak emission (except **2F** and **6F**, see below) in a polar environment. This difference is governed mainly by the higher non-radiative decay rate constant k_{nr} in polar media, whereas the radiative rate constant k_r is independent of the polarity. The k_{nr} increases as the length of the helicene increases, whereas k_r remains almost unchanged, and thus the Φ_F decreases from [6]helicene **3F** ($\Phi_F = 0.115$) to [9]helicene **8F** ($\Phi_F = 0.029$). The fluorescence lifetimes (5–10 ns) are higher than in the aceno[*n*]helicenones 1 A-8A (2–4 ns) but lower than for the parent helicenes (10–15 ns).[25] Annulation of one benzene ring in the linear direction of the fluorenone affects considerably the photophysical

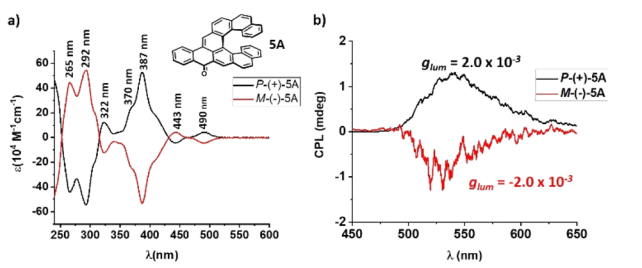

Fig. 6 (a) Circular dichroism spectra of **5A** in DCM. (b) CPL spectra of (*P*) and (*M*) enantiomers of **5A** in DCM, ($c \approx 1 \times 10^{-5}$ M).

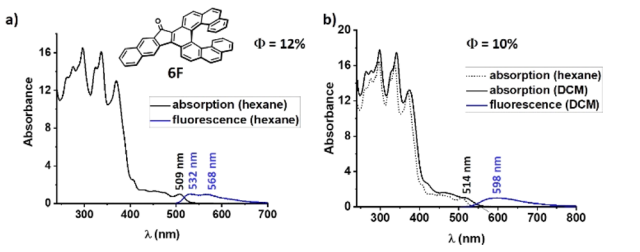

Fig. 7 (a) Absorption and emission spectra of **6F** in nonpolar hexane. (b) Absorption and emission spectra of **6F** in polar DCM, ($c \approx 1 \times 10^{-5}$ M).

Table 2 The evolution of the photophysical properties upon elongation of the helix

Helicene	$\lambda_{(onset)}$ [nm] hexane	$\lambda_{(em)}$ [nm] DCM	B_{CPL}[c] ($g_{lum} \times 10^{-3}$)[d] DCM	Φ_F[e] (%) hexane/DCM/ACN	E_{HOMO}[f] [eV]	E_{LUMO}[g] [eV]
1F	535	545[a]		5.5/0.6/0.6	−5.8	−3.43
2F	515	521[b]		22.0/13.9/13.5	−5.87	−3.43
3F	534	545[a]		11.5/1.9/1.85	−5.79	−3.42
4F	549	557[a]		6.9/1.07/0.76	−5.68	−3.37
5F	549	560[b]		4.22/0.55/0.61	−5.71	−3.4
6F	528	532[b]	8.8 (+3.9/−3.6)	12.0/10.0/8.4	−5.76	−3.37
7F	560	575[a]		6.2/0.86/0.72	−5.69	−3.43
8F	588	600		2.9/0.38/0.70	−5.62	−3.44

[a] Wavelength of excitation 330 nm. [b] Wavelength of excitation 336 nm. [c] Brightness calculated as $B_{CPL} = \epsilon_{max} \times \Phi_{PL} \times |g_{lum}|/2$. [d] Concentration $c \approx 1 \times 10^{-5}$ M. [e] Measured at room temperature ($c \approx 1 \times 10^{-6}$ M). [f] Calculated as $E_{HOMO} = E_{LUMO} - E_{(0,0)}$. [g] Calculated using the equation $E_{LUMO} = -[E'_{red/onset} + 4.8]$ referenced against Fc/Fc^+.[24]

properties. Primarily, extension of **1F** and **5F** by one benzene ring leads to a blue-shift of the absorption by 20 nm (**1F** → **2F**, 535 nm → 515 nm; **5F** → **6F**, 549 nm → 528 nm, Table 2). This hypsochromic shift is due to both electronic and geometric effects. The electronic effect includes an increase of the LUMO energy caused by a supplementary electron donation from the new annulated ring to the carbonyl group. This extra electron density lowers the carbonyl (C=O) bond strength, as confirmed by infrared spectroscopy. The stretching frequencies of **1F** (ν_{CO} = 1700 cm^{-1}) and **5F** (ν_{CO} = 1700 cm^{-1}) are higher than those of **2F** (ν_{CO} = 1692 cm^{-1}) and **6F** (ν_{CO} = 1692 cm^{-1}), respectively. The length and thus the bond strength of the carbonyl group of **5F** and **6F** (**5F** = 1.220 Å *vs.* **6F** = 1.226 Å) was probed by single crystal XRD which confirmed the donating effect of the extra benzene ring. Interestingly, the one benzene ring annulation (**5F** → **6F**) significantly increases the distance of the two terminal rings in solid state (distance between the centroids of the overlapping benzene rings A–C, $5F_{A-C}$ = 3.814 Å, $6F_{A-C}$ = 4.047 Å, for details, see ESI† page S165) of the helicene backbone, with a disruptive effect on the through-space conjugation. However theoretical calculations do not show such a large distance between the terminal rings ($5F_{A-C}$ = 3.71 Å; $6F_{A-C}$ = 3.70 Å, calculated at the level wB97X-D/Def2SVP using Gaussian 16 Rev C.02). The extra benzene ring has a strong effect on the Φ_F both in nonpolar (Φ_F in hexane of **1F** → **2F**, 0.055 → 0.22 and **5F** → **6F**, 0.042 → 0.12) and in polar environment (Φ_F in DCM of **1F** → **2F**, 0.006 → 0.139 and **5F** → **6F**, 0.006 → 0.10). The oscillator strength was only slightly improved, but the non-radiative decay rate constant k_{nr} was drastically reduced in both nonpolar and polar media, leading to an increased Φ_F. These fluoreno[*n*]helicenes show a regular trend of decreasing gap ($E_{0,0}$) with increasing length of the helicene. The decrease of the gap, when going from fluoreno[6]helicene **3F** to fluoreno[6]helicene **8F** is less prominent ($E_{0,0}$ **3F–8F** = 0.19 eV) than for the homologous aceno[*n*]helicenones **3A** and **8A** ($E_{0,0}$ **3A–8A** = 0.25 eV). **1F–8F** do not exhibit phosphorescence even at 5K. This can be explained by their energy-level diagram profiles. All the diagrams of **1F–8F** have similar profiles and show that there is only one triplet state below the lowest excited state S_1. All the higher triplet states are well above the S_1. Thus, the ISC from the S_1 to T_2 and to higher triplet states is endothermic and suppressed at low temperatures. T_1 is the only triplet state which could participate in ISC from S_1. However, the relatively high energy difference (E_{S1-T1} > 0.4 eV) and similar nature of S_1 and T_1 states (spin–orbit-coupling, SOC, in case of **6F** = 0.143 and **7F** = 0.124) renders ISC inefficient. Therefore, the internal conversion from S_1 to S_0 becomes the only nonradiative deactivation channel. Based on our experiments and theoretical calculations, the ΔE_{S0-T1} gap systematically decreases as the length of the helicene part increases, as the energy of the triplet state is associated with conjugation length (see ESI† page S158). The energy of T_1 is decreasing to the same extent as the energy of S_1, thus the energy gap ΔE_{S1-T1} remains constant as the length of the helix increases. Benzannulation of the fluorene part lifts the S_1 but has only a minuscule effect on the T_1, thus there is an increase of the ΔE_{S1-T1} gap. CV measurements were performed to determine the electrochemical properties of **1F–8F**. All exhibit two reversible reduction waves. From the onset of the reduction wave, the LUMO energy levels of **1F–8F** were calculated. The HOMO energy levels were calculated from the absorption onset wavelength, *i.e.* from the optical gap (for details, see ESI† Table S2 page S157).

Chiroptical properties of fluoreno[7]helicene 6F

We could separate the enantiomers of fluoreno[7]helicene **6F** by HPLC on a chiral stationary phase column. The absolute configurations were assigned by CD spectroscopy with the aid of TD-DFT calculations. The first eluting fraction was assigned as the *P*-(+) and the second one as the *M*-(−) enantiomer. The enantiomers give perfectly mirror-symmetric CD spectra (Fig. 8) with opposite Cotton effects, with the maximum at 263 nm and a large dissymmetry factor (***P*-6F**, $g_{abs} = -5.7 \times 10^{-3}$). The longest absorption band at 434–562 nm, with $g_{abs} = -2.5 \times 10^{-3}$ (***P*-6F**), is assigned to the $S_0 \rightarrow S_1$ transition. The CPL spectra are mirror-symmetric as well, with relatively high g_{lum} = 3.9/-3.8 $\times 10^{-3}$, and the sign of the CPL matches that of the CD. The absorption and luminescence dissymmetry factors g_{abs} and g_{lum} are not affected by the polarity of the environment. On the basis of our calculations, the g_{lum} of the fluoreno-family is decreasing as the helix increases (**3F** → **5F** → **7F** → **8F**, $g_{lum} = 6.3 \times 10^{-3} \rightarrow 6.9 \times 10^{-3} \rightarrow 5.7 \times 10^{-3} \rightarrow 2.5 \times 10^{-3}$) which is the opposite of the aceno[*n*]helicenones **1A–8A**. Benzannulation

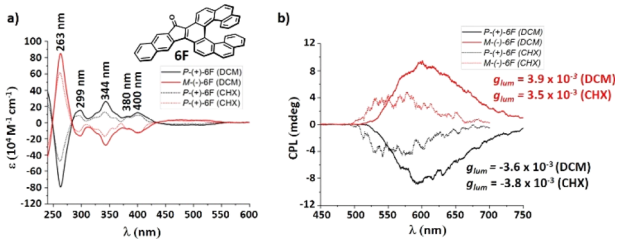

Fig. 8 (a) Circular dichroism spectra of **6F**. (b) CPL spectra of (*P*) and (*M*) enantiomers of **6F**, ($c \approx 1 \times 10^{-5}$ M).

negatively influences the luminescence dissymmetry factor (**1F** → **2F** $g_{lum} = 7.7 \times 10^{-3} \rightarrow 4.9 \times 10^{-3}$; **5F** → **6F** $g_{lum} = 6.9 \times 10^{-3} \rightarrow 4.2 \times 10^{-3}$). The specific rotation of ***P*-6F** (+434 deg cm^2 g^{-1}) is significantly lower when compared to the parent carbo[7]helicene (±6200 deg cm^2 g^{-1})[32] or aceno[7]helicene ***P*-6A** (+2014 deg cm^2 g^{-1}). Three of the structures **5F**, **6F** and **8F** were unambiguously confirmed by single-crystal XRD analysis. In all cases, suitable crystals were grown from a racemic solution by slow evaporation of cyclohexane : DCM (1 : 1). The interplanar angles of the two terminal rings A and C are 25.2°, 30.5° and 15.7°, respectively (for details, see ESI† page S168).

Conclusions

In summary, we have made a comprehensive investigation about the structure–property relationship of carbonyl-aceno[*n*]helicenes **1A–8A** and carbonyl-fluoreno[*n*]helicenes **1F–8F**. We analyzed their structural, photophysical and chiroptical properties using NMR, CV, ECD, CPL and single crystal XRD, and the experimental results were confirmed by TD-DFT calculations. We have shown that the installation of a carbonyl group at the periphery of the carbo[*n*]helicene backbone improves greatly the photophysical properties. The aceno[*n*]helicenones **1A–8A** and fluoreno[*n*]helicenes **1F–8F** are much more emissive than the parent helicenes. This highlights the limitations of the generally accepted rule of nonemissivity of aromatic carbonyl compounds. Elongation of the helix leads to convergent evolution of the HOMO–LUMO energy gap for both families. Elongation of the acene part leads to an expected red-shift, but benzene ring annulation on the fluorenone part causes a counterintuitive blue shift. This divergent evolution of the energy gaps was corroborated by TD-DFT calculations. CD and CPL have shown large absorption and luminescence dissymmetry factors g_{abs} and g_{lum}, which are dependent on the length of the acene/fluorenone and helicene part. g_{abs} and g_{lum} substantially increase with the helical length (*n*) in the family of aceno[*n*]helicenones **1A–8A**. In contrast, our theoretical calculations show that the g_{lum} of fluoreno[*n*]helicenes **1F–8F** is decreasing as the length of the helix increases.

Data availability

The data are provided in the ESI.†

Author contributions

M. S., A. J., L. S. and A. R. performed all the synthetic work. L. S. and A. B. performed CD, CPL and CV characterization. M. B., B. K. and O. M. performed all the photophysical studies. I. D. did all theoretical calculations. Y. N. calculated dissymmetry factors (g_{abs} and g_{lum}). A. J. wrote the article with assistance of H. B. and I. D.

Conflicts of interest

There are no conflicts to declare.

Acknowledgements

Calculations were performed at the Interdisciplinary Center for Mathematical and Computational Modeling (ICM) University of Warsaw under computational allocation G91-1402. The authors thank Reiko Oda for using her CD and CPL facility, Ivo Starý and Irena Stará for using their chiral HPLC facility. Mathieu Rouzieres is thanked for his drawings. Andre Gourdon is thanked for his comments. This work was supported by the University of Bordeaux, the Région Nouvelle Aquitaine, Quantum Matter Bordeaux (QMBx) and the Centre National de la Recherche Scientifique (CNRS). This work was supported by the Czech Science Foundation (Reg. No. 20-23566S) and the Institute of Organic Chemistry and Biochemistry, Czech Academy of Sciences (RVO: 61388963). This work was partly supported by JSPS KAKENHI grant numbers JP21H01924 and JP23H03810, and JST *via* the ERATO grant JPMJER1903 and the CREST grant JPMJCR2001. The computation was partly performed using Research Center for Computational Science, Okazaki, Japan (Project: 23-IMS-C119). Support was also provided by the Institute for Chemical Reaction Design and Discovery (ICReDD), established by the World Premier International Research Initiative (WPI), MEXT, Japan.

Notes and references

1 C. M. Marian, *Annu. Rev. Phys. Chem.*, 2021, **72**, 617–640.
2 M. Baba, *J. Phys. Chem. A*, 2011, **115**, 9514–9519.
3 S. Aloïse, C. Ruckebusch, L. Blanchet, J. Réhault, G. Buntinx and J.-P. Huvenne, *J. Phys. Chem. A*, 2008, **112**, 224–231.
4 M. Alías-Rodríguez, C. De Graaf and M. Huix-Rotllant, *J. Am. Chem. Soc.*, 2021, **143**, 21474–21477.
5 T. Kobayashi and S. Nagakura, *Chem. Phys. Lett.*, 1976, **43**, 429–434.
6 J. Crassous, I. G. Stará and I. Starý, *Helicenes: Synthesis, Properties and Applications*, Wiley, 1st edn, 2022.
7 J. B. Birks, D. J. S. Birch, E. Cordemans and E. Vander Donckt, *Chem. Phys. Lett.*, 1976, **43**, 33–36.
8 M. Sapir and E. V. Donckt, *Chem. Phys. Lett.*, 1975, **36**, 108–110.
9 J. Crassous, in *Circularly Polarized Luminescence of Isolated Small Organic Molecules*, ed. T. Mori, Springer Singapore, Singapore, 2020, pp. 53–97.

10 K. Dhbaibi, L. Abella, S. Meunier-Della-Gatta, T. Roisnel, N. Vanthuyne, B. Jamoussi, G. Pieters, B. Racine, E. Quesnel, J. Autschbach, J. Crassous and L. Favereau, *Chem. Sci.*, 2021, **12**, 5522–5533.
11 K. Dhbaibi, L. Favereau, M. Srebro-Hooper, M. Jean, N. Vanthuyne, F. Zinna, B. Jamoussi, L. Di Bari, J. Autschbach and J. Crassous, *Chem. Sci.*, 2018, **9**, 735–742.
12 H. Kubo, T. Hirose, T. Nakashima, T. Kawai, J. Hasegawa and K. Matsuda, *J. Phys. Chem. Lett.*, 2021, **12**, 686–695.
13 Z. Qiu, C.-W. Ju, L. Frédéric, Y. Hu, D. Schollmeyer, G. Pieters, K. Müllen and A. Narita, *J. Am. Chem. Soc.*, 2021, **143**, 4661–4667.
14 P. Izquierdo-García, J. M. Fernández-García, S. Medina Rivero, M. Šámal, J. Rybáček, L. Bednárová, S. Ramírez-Barroso, F. J. Ramírez, R. Rodríguez, J. Perles, D. García-Fresnadillo, J. Crassous, J. Casado, I. G. Stará and N. Martín, *J. Am. Chem. Soc.*, 2023, **145**, 11599–11610.
15 Y. Sawada, S. Furumi, A. Takai, M. Takeuchi, K. Noguchi and K. Tanaka, *J. Am. Chem. Soc.*, 2012, **134**, 4080–4083.
16 H. Oyama, M. Akiyama, K. Nakano, M. Naito, K. Nobusawa and K. Nozaki, *Org. Lett.*, 2016, **18**, 3654–3657.
17 R. J. Malone, J. Spengler, R. A. Carmichael, K. Ngo, F. Würthner and W. A. Chalifoux, *Org. Lett.*, 2023, **25**, 226–230.
18 L. Wang, L. Duan, B. Hong and Z. Gu, *Org. Lett.*, 2023, **25**, 1912–1917.
19 K. Murayama, Y. Shibata, H. Sugiyama, H. Uekusa and K. Tanaka, *J. Org. Chem.*, 2017, **82**, 1136–1144.
20 J. Feng, L. Wang, X. Xue, Z. Chao, B. Hong and Z. Gu, *Org. Lett.*, 2021, **23**, 8056–8061.
21 R. P. Kaiser, D. Nečas, T. Cadart, R. Gyepes, I. Císařová, J. Mosinger, L. Pospíšil and M. Kotora, *Angew. Chem., Int. Ed.*, 2019, **58**, 17169–17174.
22 T. Cadart, D. Nečas, R. P. Kaiser, L. Favereau, I. Císařová, R. Gyepes, J. Hodačová, K. Kalíková, L. Bednárová, J. Crassous and M. Kotora, *Chem.–Eur. J.*, 2021, **27**, 11279–11284.
23 I. G. Stará and I. Starý, *Acc. Chem. Res.*, 2020, **53**, 144–158.
24 R. M. G. Rajapakse, D. L. Watkins, T. A. Ranathunge, A. U. Malikaramage, H. M. N. P. Gunarathna, L. Sandakelum, S. Wylie, P. G. P. R. Abewardana, M. G. S. A. M. E. W. D. D. K. Egodawele, W. H. M. R. N. K. Herath, S. V. Bandara, D. R. Strongin, N. H. Attanayake, D. Velauthapillai and B. R. Horrocks, *RSC Adv.*, 2022, **12**, 12089–12115.
25 E. Vander Donckt, J. Nasielski, J. R. Greenleaf and J. B. Birks, *Chem. Phys. Lett.*, 1968, **2**, 409–410.
26 Z. Sun and J. Wu, *Aust. J. Chem.*, 2011, **64**, 519.
27 R. Einholz, T. Fang, R. Berger, P. Grüninger, A. Früh, T. Chassé, R. F. Fink and H. F. Bettinger, *J. Am. Chem. Soc.*, 2017, **139**, 4435–4442.
28 P. Ribar, L. Valenta, T. Šolomek and M. Juríček, *Angew. Chem., Int. Ed.*, 2021, **60**, 13521–13528.
29 J. Schöntag, M. Ströbele, H. Schubert and H. F. Bettinger, *Eur. J. Org Chem.*, 2024, **27**, e202301161.
30 Y. Y. Pan, J. Huang, Z. M. Wang, D. W. Yu, B. Yang and Y. G. Ma, *RSC Adv.*, 2017, **7**, 26697–26703.
31 Y. Nakai, T. Mori and Y. Inoue, *J. Phys. Chem. A*, 2012, **116**, 7372–7385.
32 K. P. Meurer and F. Vögtle, in *Organic Chemistry*, Springer-Verlag, Berlin/Heidelberg, 1985, vol. 127, pp. 1–76.